Comparative analysis of bridge cables with concave fillets

Burlina, Celeste; Georgakis, Christos T.; Larsen, Søren V.; Egger, Philipp

Publication date:
2016

Document Version
Peer reviewed version

COMPARATIVE ANALYSIS OF BRIDGE CABLES WITH CONCAVE FILLETS

1st Celeste Burlina[+1], 2nd Christos T. Georgakis[+2], 3rd Søren V. Larsen[+3] and 4th Philipp Egger[+4]
[+1,2]Technical University of Denmark, Copenhagen ,Denmark
[+3]FORCE Technology, Copenhagen, Denmark
[+4]VSL International Ltd., Knizö, Switzerland

In this paper the aerodynamic performance of two new cable surfaces with concave fillets are examined and compared to cables with traditional helically filleted, plain and pattern indented surfaces. To this end, an extensive wind-tunnel campaign was undertaken to measure the aerodynamic static force coefficients up to the super-critical Reynolds number range and rain-rivulet suppression ability. Flow visualizations tests were performed to better understand the structure and development of the wake. Both innovations outperform traditional surfaces in terms of rain-rivulet suppression thanks to the ability of the concave shaped fillet to act as a ramp for the incoming rain-rivulet. Furthermore both innovations are able to suppress vortex shedding at low Reynolds numbers, in contrast to the other cable surfaces tested. Moreover the innovation with the staggered surface shows an early reduction of the drag force while maintaining a zero lift up to the super-critical range.

Keyword: cable aerodynamics, concave fillets, rain rivulet suppression, force coefficients, flow visualizations.

1. INTRODUCTION

In order to reduce wind-induced vibrations on bridge stay cables, such as rain wind induced vibrations (RWIV) and dry galloping, bridge cable manufacturers have introduced cable surface modifications on the protective high-density polyethylene (HDPE) pipes. These modifications come mainly in the form of helical fillets, extensively used in Europe and North America, and in the form of dimples, used predominantly in Asia. The main purpose of these modifications is rain-rivulet impedance, since the presence of one or more longitudinally running rivulets on the cable surface is considered one of the major causes of the initiation of RWIV. Nevertheless, the introduction of helical fillets and dimples has not completely eliminated RWIVs, often leading bridge owners to the installation of cable vibration dampers or cross-ties (Kleissl and Georgakis, 2013). Previous research (Yagi, 2011 and Kleissl and Georgakis, 2013) shows that by modifying the shape, alignment and configuration of the protuberances on the HDPE tube, it is possible to eliminate or further reduce the RWIVs, together with a reduction in drag force. Drag force represents more than 50% of the overall horizontal wind load on long span bridges (Gimsing and Georgakis, 2012). In particular, cable surface modifications in the form of a concave fillet, studied by Kleissl and Georgakis (2013), were found to outperform traditional surfaces, showing similar aerodynamic coefficients, compared to a traditional helical fillet and dimpled surface despite a significant increase in the fillet height.

As a result, the objective of the present study is to examine the aerodynamic performance and to further understand the behavior of innovative bridge cable surfaces with concave fillets, and to compare this performance with that of a cable with a traditional helical fillet, dimpled and plain surface. In particular, a better understanding of the flow structure and development of the near wake of the bridge cable makes it possible to investigate the flow mechanisms initiated and to employ further manipulation and improvement of the concave fillet for drag reduction, while at the same time guaranteeing optimal performance in terms of rain-rivulet suppression.

To this end, an extensive wind-tunnel test campaign was performed at the Climatic Wind Tunnel

[+1]celebur@byg.dtu.dk, [+2]cg@byg.dtu.k, [+3]svl@force.dk, [+4]philipp.egger@vsl.com

(CWT) at FORCE Technology (Denmark). A first set of tests was run in static conditions, in order to evaluate aerodynamic coefficients for different cable surfaces from the sub-critical to the post-critical Reynolds number range. In a second stage, rain rivulet suppression and flow visualization tests on the same samples were undertaken at different wind velocities in the sub-critical Reynolds number range. These investigations were performed in order to investigate the dependencies of the shape of the concave fillet on the suppression of the rain-rivulet and on the development of the wake in relation to the resultant drag coefficient and initiation of vortex shedding.

2. MODELS

The models tested were full-scale samples of high density polyethylene (HDPE) tubing with an outer diameter of 160mm (excluding fillet). Different cable surfaces were tested. Two innovative profiles that involve the application of concave protruding fillets were tested. The fillet cross section has a trapezoidal shape with concave sides and a height of 6.5mm. In the first model, which will be subsequently referred as Innovation 1, the fillets replicate the typical arrangement of current stay cables with helical fillets, with a pitch angle of 45^{o} and a spiral distance of 251mm. In the second model, Innovation 2, the fillets are arranged laterally in a staggered helical pattern with a pitch angle of 30^{o} and spacing between the fillets of 20mm. For comparison reasons plain, dimpled and traditional helically filleted cable surfaces were also tested.

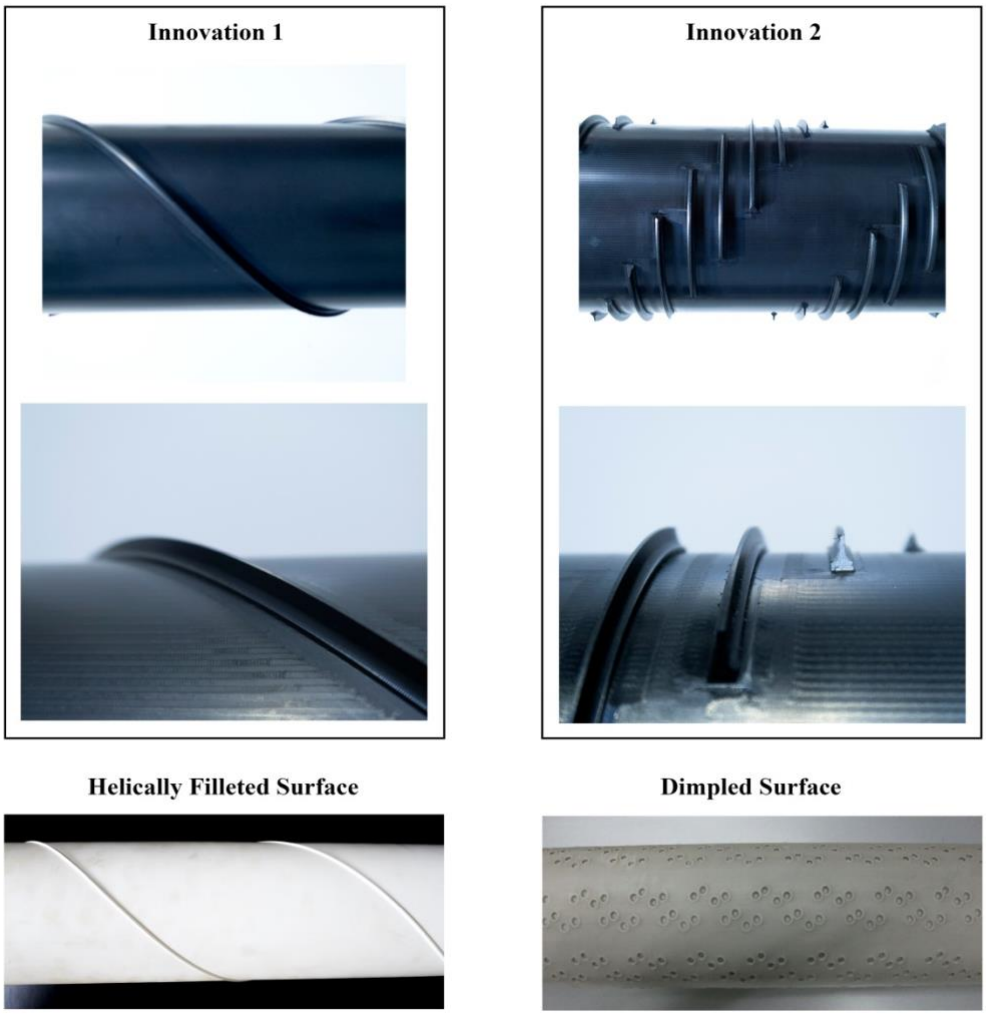

Figure 1: Cable sample models

[+1]celebur@byg.dtu.dk, [+2]cg@byg.dtu.k, [+3]svl@force.dk, [+4]philipp.egger@vsl.com

3. EXPERIMENTAL WORK

The cables section prototypes were placed horizontally in the wind tunnel cross section, resulting in a near two-dimensional flow normal to the cable section, for both static and flow visualization set-ups. The drag and lift forces were measured up to super-critical Reynolds number range, using 6DOF force transducers (AMTI MC3A-500) at either end. The two force transducers were installed between the cable model and supporting cardan joints. The length of the models was 1.42m, resulting in an aspect ratio of 8.9:1. The blockage ratio for the cable model ratio for the cable model was 8% and thus the drag coefficients have been corrected using the Maskel III method, according to Cooper et al. (1999). For each tested configuration, the drag C_D and the lift C_L coefficients were calculate, based on the averaged along-wind and across-wind forces respectively, normalized by the along-wind flow velocity:

$$C_D = \frac{F_D}{\frac{1}{2}\rho U^2 LD} \tag{1}$$

$$C_L = \frac{F_L}{\frac{1}{2}\rho U^2 LD} \tag{2}$$

where F_D is the along-wind force and F_L is the across-wind component, U is the mean wind velocity, L is the effective length of the cable, D the outer diameter and ρ the air density, taken here as 1.25kg/m^3.

During the flow visualization tests, smoke particles were added into the flow to trace the fluid motion. With smoke particles in the order of 0.2μm, it can be assumed that the particles follow the streamline of the flow. Due to dispersion of the particles at high wind velocities, tests were run up to the sub-critical Reynolds number range limit. In order to visualize a slice of the fluid flow pattern, the particles were illuminated with sheet of laser light.

Rivulet suppression tests were performed with the cable declining along the wind direction at a relative cable-wind angle of 45º (See Kleissl and Georgakis 2013). A plain surface cable section was used to make up the first top half of the model length, in order to facilitate the formation of the upper and lower rivulet, while the different cable surfaces section were used to make up the second half of the model length. All tests were repeated for 8m/s and 14m/s, which are the representative values for the upper and lower velocity range for RWIV. The dimpled surface was not tested for rivulet suppression due to incompatibility of the set-up.

(a) (b)

Figure 2: Rivulet suppression Set-up (a) and Static and Flow Visualization Set-Up (b)

[+1]celebur@byg.dtu.dk, [+2]cg@byg.dtu.k, [+3]svl@force.dk, [+4]philipp.egger@vsl.com

4. RESULTS AND DISCUSSION

(1) Force Coefficients

The drag and lift coefficients obtained for each of these tested models are shown in Figure3. It can be noted that the plain cable's aerodynamic forces are in agreement with the expectations for a smooth cylinder of this kind, entering the critical Reynolds number region for Re = 2.2 - 2.6 x 10^5 and reaching a minimum value of drag coefficient of 0.4 in the supercritical state. In the same interval the lift coefficient shows a relatively large value, due to the formation of a single separation bubble.

The traditional helically filleted surface and Innovation 1 experience the same drag force in the sub-critical Reynolds number range, while after the transition to the post-critical range, the traditional fillet experiences a lower drag force due to a more accentuated drag transition in the Reynolds number range between 2.0 and 2.6 x 10^5. Despite the same arrangement of the fillet for the surfaces in question, the higher drag coefficient in the post-critical Reynolds range for Innovation 1 can be attributed to the higher profile of the fillet directly facing the incoming flow, which acts as a fixed ramp and separation point and thus resulting in a wider wake.

On the other hand, Innovation 2 and the dimpled surface show an earlier reduction in the drag force in the sub-critical Reynolds range and exhibit a more smooth and prolonged transition which starts at a lower Reynolds number between 0.8 - 1.0 x 10^5 and enters the post-critical state at a Reynolds number of 2.0 x 10^5. The early flow transition for the dimpled surface cable agrees well with what has been observed for circular cylinders with uniform high roughness, which easily triggers turbulence ensuring a near constant super-critical drag (Miyata et al. 1994 and Hojo et al. 1995). For Innovation 2, it is hypothesized that the early transition and the subsequent constant super-critical drag is the result of the fact that the circumferential orientation of the fillets reduces the drag penalty, whilst triggering turbulence at the boundary layer and introducing counter rotating vortices.

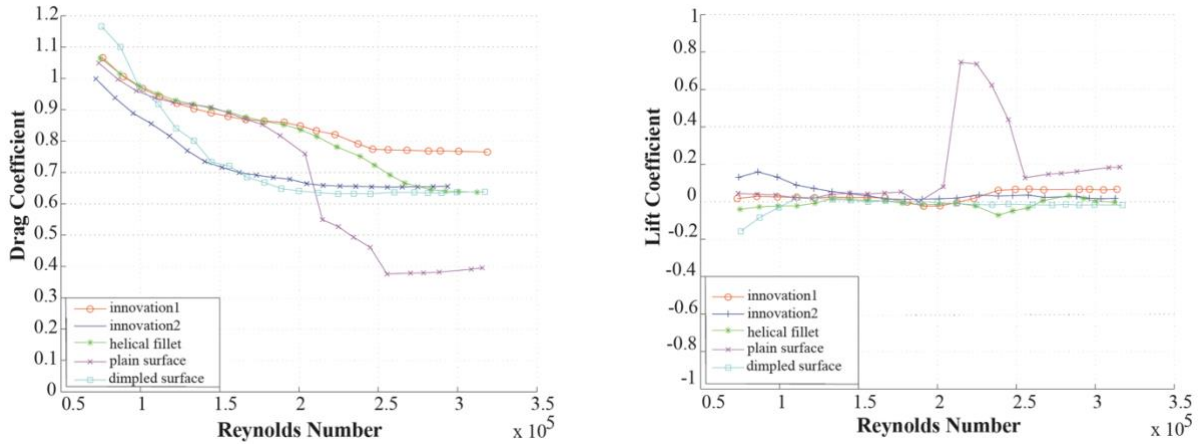

(a) (b)

Figure 3: Drag coefficients (a) and Lift coefficients (b) comparison.

Concerning the lift force, apart from the plain cable surface as mentioned before, the other four cable surfaces experience an almost zero lift along the whole range of wind velocities tested (Figure 3b) This is most likely due to the ability of all the surface modifications to generate variations in the flow and separation lines along the length of the cable. These variations, as largely reported in previous studies, are the result of enhanced vorticities and counter rotated vortices for the dimpled surface (Miyata et al., 1994) and of periodic structures in the spanwise direction with localized increased streamwise vorticities and elongations of the vortex formation region for the traditional helical fillet (Nebres and Batill, 1993).

[+1]celebur@byg.dtu.dk, [+2]cg@byg.dtu.k, [+3]svl@force.dk, [+4]philipp.egger@vsl.com

(2) Fluctuating Lift Forces

A frequency analysis of the unsteady cross-stream force (fluctuating lift) was undertaken. With the particular cross flow test set up employed, the fluctuations of the total lift force on the model can be determined. The frequency distributions of the lift force are determined using a Fast Fourier Transformation (FFT) to compute the power spectral density (PSD) of the lift coefficient. The PSD is computed for each of the flow velocities tested. The discrete number of flow velocity-specific spectra is then expanded into a two-dimensional contour plot, as seen in Figure 4, for each of the cable models. The Strouhal number is computed for all five cables ($St = f_s D/U$, where f_s is the frequency of vortex shedding). The increased PSDs at around 30 and 35Hz can be explained as the incidences of model resonance. The linear trend identifying vortex shedding disappears around a Reynolds number of 2.0 and 2.2 x 10^5 for the plain cable and the traditional helically filleted cable respectively. These values correspond for both surfaces to the flow transition from sub-critical to the post-critical Reynolds range. The same linear behavior disappears at much lower Reynolds numbers for Innovation 1 and 2. Here this occurs at Reynolds number of 1.5 x 10^5 for both innovations, which correspond to the smooth and prolonged drag transition for Innovation 1 and the entrance in the super-critical range for Innovation 2. On the other hand, the vortex shedding remains throughout the whole range of tested velocities for the dimpled cable surface, despite the early flow transition at a Re = 0.8 - 1.0 x 10^5, as experienced also by Innovation 2. Furthermore, a significantly higher Strouhal number of 0.28 is determined for the dimpled surface compared to the other samples, which were founded to have a Strouhal number of 0.20.

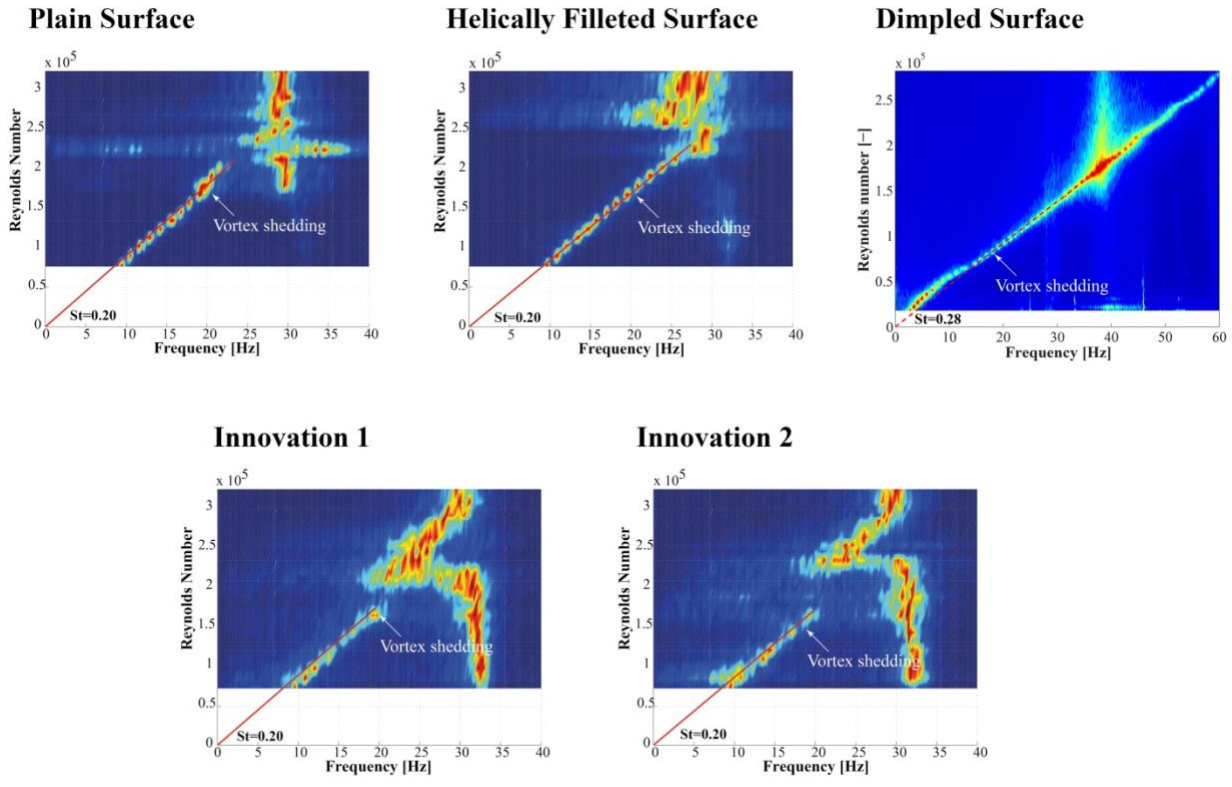

Figure 4: Normal flow lift coefficient PSD for different cable surfaces.

As a result, both Innovation 1 and 2 are able to suppress vortex shedding formation at much lower wind velocities than a traditional helical fillet or dimpled surface. In particular Innovation 2, which experiences the same drag reduction showed by the dimpled surface, is able to suppress vortex shedding in the same range as the transition to the super-critical regime.

[+1]celebur@byg.dtu.dk, [+2]cg@byg.dtu.k, [+3]svl@force.dk, [+4]philipp.egger@vsl.com

(3) Rivulet supression

As found in by previous studies by Kleissl and Georgakis (2013) the critical range of velocities for the formation of both upper and lower rain-rivulets is between 7 – 15 m/s. Outside this range, the upper rivulet does not form, as either gravity or the wind loading become dominant. As RWIVs typically occur within this range, the presence of the upper rivulet is considered particularly critical for the initiations of these vibrations.

Figure 5 shows the rain rivulet suppression ability of the tested cable surfaces. The traditional helical fillet is able to reduce the size of the rain rivulet along the length of the cable but it is not able to completely suppress. Innovation 1 and Innovation 2 experience a complete suppression of the upper and lower rivulets at both velocities tested. The particular shape of the concave fillet acts as a ramp, blocking the formation of the upper and lower rivulet along the whole length of the cable. In particular it was noticed that this is mainly due to the concavity of the fillet and its sharp top edge.

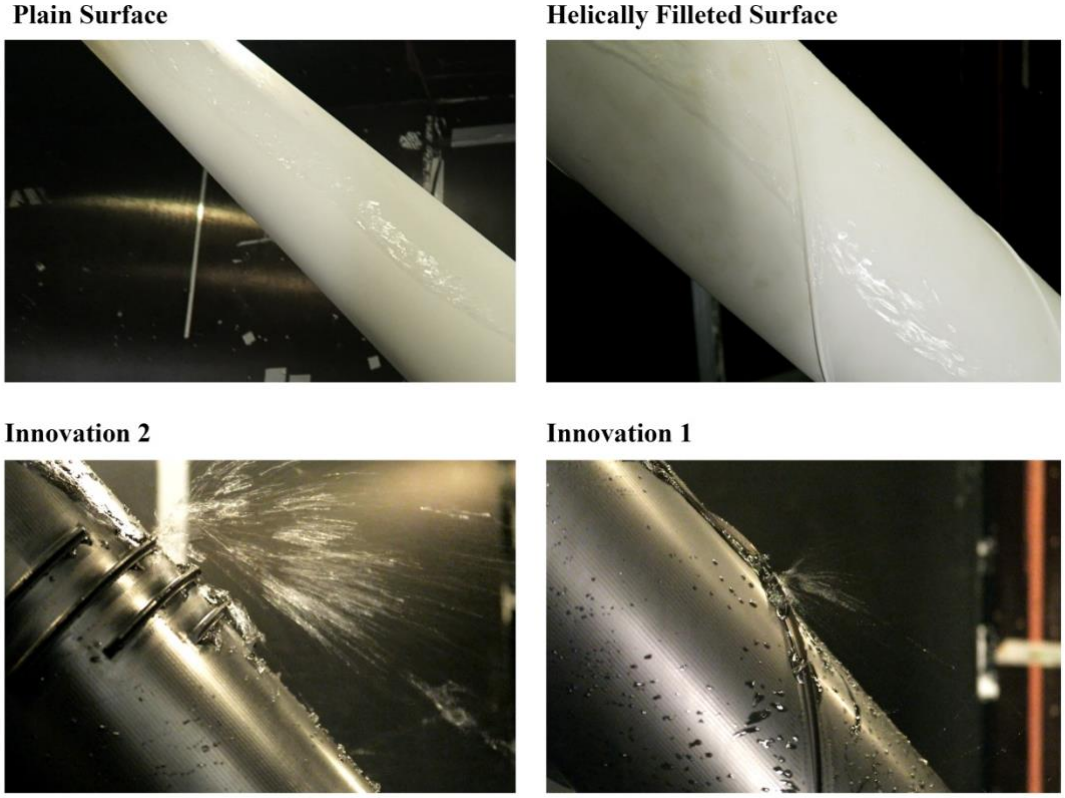

Figure 5: Rivulet suppression ability for different cable surfaces.

(4) Flow Visualization

a) Far-wake flow visualization

The flow visualizations of the far-wake flow structure for all the five cables tested, whilst positioned normal to the flow, are shown in Figure 6. As previously discussed, when analyzing the power spectral density (PSD) of the lift coefficient, at Re = 0.6 x 10^5 all five samples experience the formation of vortex shedding, although this is disturbed in the case of traditional helical fillet, Innovation 1 and Innovation 2, due to the generation of three-dimensional flow structures introduced by the presence of the fillets, as they generate uncorrelated fluctuations along the span of the cylinder (Zdravkovich, 1981 and Nebres and Batill 1993).

At Re = 1.5 x 10^5 all cables exhibits a reduction of the vortex shedding formation, which is particularly reduced for Innovation 1 and 2, due to an increase of the disturbance created by the concave fillet compared to the traditional rounded shape of the helical fillet. This behavior is particularly accentuated in Innovation 2, where the staggered configuration of the fillet around the circumference is able to enhance turbulences at the boundary layer. On the other hand, the dimpled surface, even though showing the same behavior as Innovation 2, is not able to suppress vortex shedding formation even after entering the post-critical regime.

[+1]celebur@byg.dtu.dk, [+2]cg@byg.dtu.k, [+3]svl@force.dk, [+4]philipp.egger@vsl.com

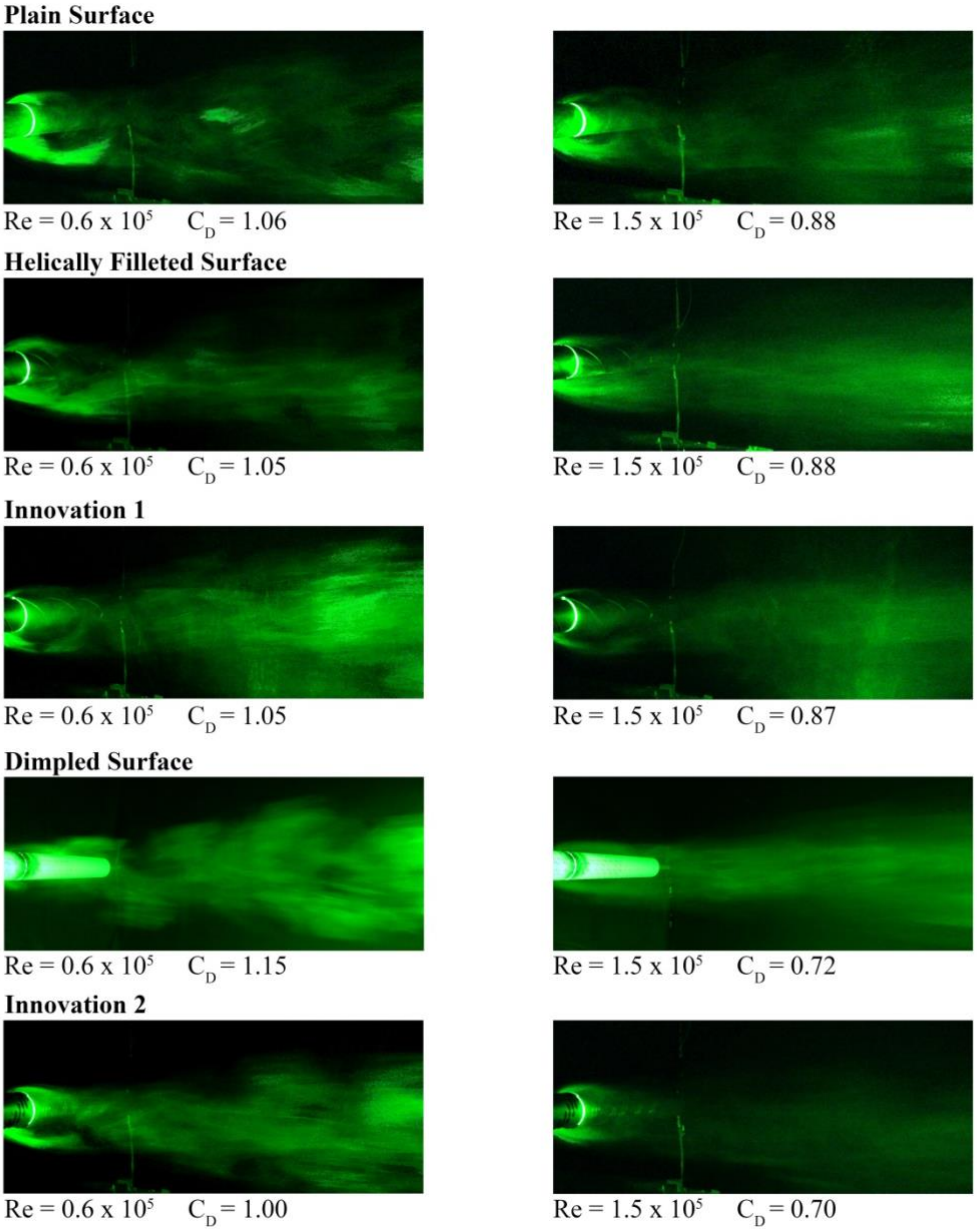

Figure 6: Far-wake flow visualization for different cable surfaces at Re = 0.6 x 10^5 and Re = 1.5 x 10^5

b) Near-wake flow visualization

The flow visualizations of the near-wake and separation mechanisms are shown in Figure 7. The near-wake photographs represent the average wake size over a full development and evolution of its structure.

From Re = 0.6 x 10^5 to Re = 1.5 x 10^5 all five samples exhibit a reduced width of their wakes, indicating also a drop in the drag coefficient. When comparing them, this behavior is particularly enhanced for the dimpled surface and Innovation 2. As we can see in Figure 7, both cable surfaces exhibit the same behavior of a plain cable in the supercritical state, where the boundary layer is fully turbulent before the separation line, resulting in a narrow wake and in a drop of the drag coefficient (Zdravkovich, 1997). This mechanism is generated artificially by the dimples in the dimpled surface and by the staggered concave fillets in Innovation 2, which are able to initiate turbulence at the boundary layer at low Reynolds number with an early transition to the post-critical state.

On the other hand, Innovation 1, exhibit a smaller reduction in the wake size and a resulting higher drag coefficient, compared to the other surfaces. The flow is governed by the presence of the concave fillet which acts as a ramp for the incoming flow, creating a fixed separation point and a subsequent enhanced

[+1]celebur@byg.dtu.dk, [+2]cg@byg.dtu.k, [+3]svl@force.dk, [+4]philipp.egger@vsl.com

vorticity. This particular behavior does not allow for a transition in the flow for increased Reynolds numbers, leading to a small reduction of the wake´s size and subsequently a small reduction of the drag coefficient also in the supercritical range. It is hypothesized that a reduction of the height of the concave fillet will result in a narrower wake and as a consequence a lower drag coefficient, whilst maintaining optimal performance in terms of rain-rivulet suppression.

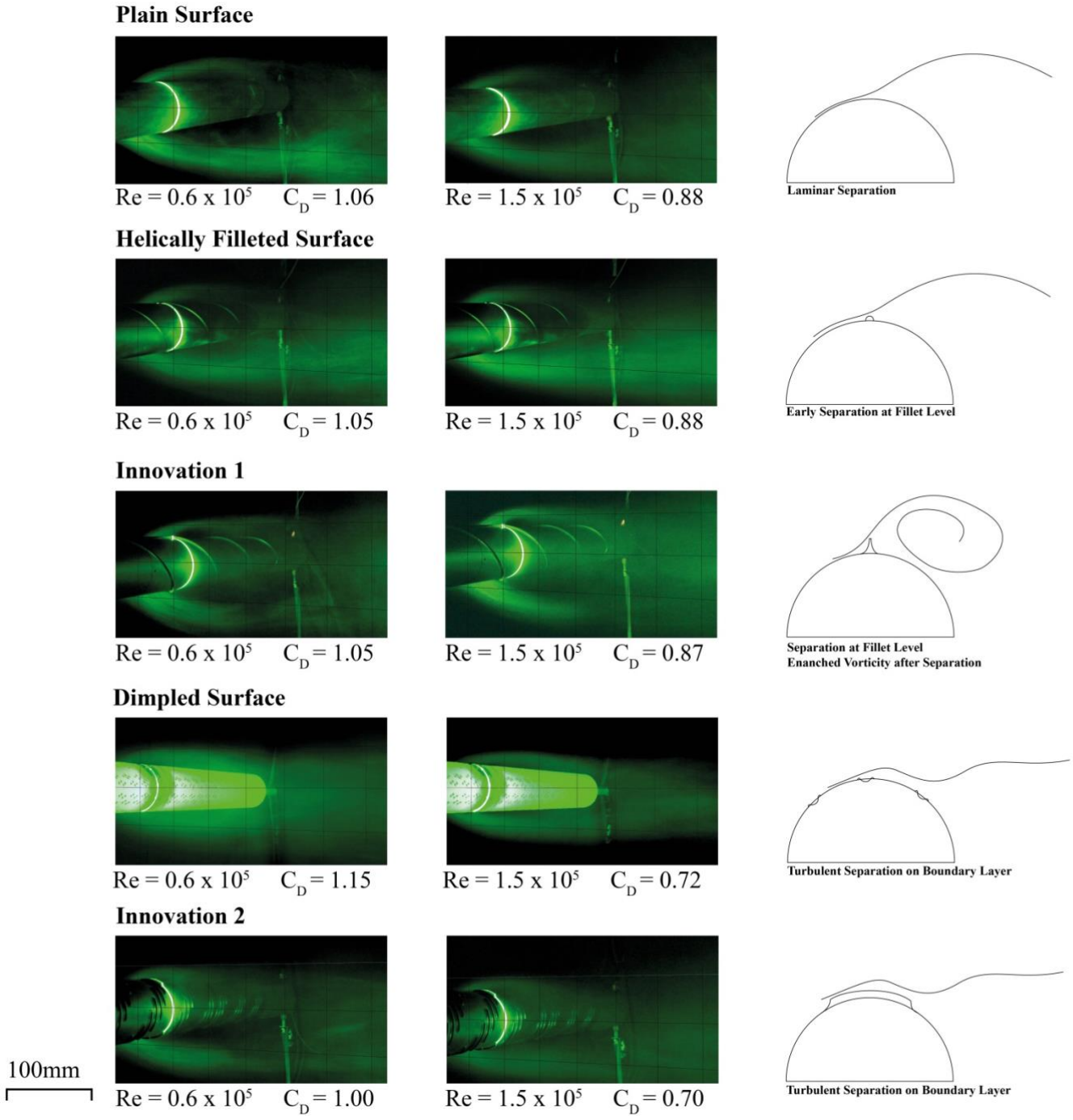

Figure 7: Near-wake flow visualization for different cable surface at Re = 0.6 x 10^5 and Re = 1.5 x 10^5

[+1]celebur@byg.dtu.dk, [+2]cg@byg.dtu.k, [+3]svl@force.dk, [+4]philipp.egger@vsl.com

5. CONCLUSIONS

Two new cable surfaces with concave fillets were wind tunnel tested for the determination of the aerodynamic coefficients, the structure of the flow's near and far-wake and for rain rivulet suppression. The results were compared with plain, dimpled and traditional helically filleted cable surfaces.

Innovation 1 and 2 outperformed in terms of rain-rivulet suppression, with a complete suppression of the upper and lower rain-rivulets at all tested velocities. This is due to the ability of the concave fillet to act as a ramp for the incoming rivulet. Moreover, they are able to suppress vortex shedding at lower Reynolds numbers compared to the other surfaces.

Both innovations maintain optimal performance in terms of aerodynamic coefficients despite a more than 100% increase of the fillet height compared to a traditional helical fillet. In particular, Innovation 2 exhibits the same behavior as a dimpled cable surface in terms of drag coefficient, showing an early transition to the super-critical and a subsequent reduction of the drag force. This is due to the ability of the staggered surface configuration to enhance turbulence at the boundary layer level. Innovation 2 is also able to suppress vortex shedding formation at lower Reynolds numbers compared to the dimpled cable surface, which maintains it up to the critical Reynolds number range.

On the other hand, Innovation 1 shows a higher drag in the super-critical range compared to the other surfaces tested. It is believed that by reducing the height of the fillet it will be possible to reduce the drag force while maintaining optimal performances in terms of rain-rivulet suppression.

ACKNOWLEDGMENT

This work would not have been possible without the generous support of VSL and FORCE Technology.

REFERENCES

1) Cooper, K., Mercke, E., Wiedemann, J. : Improved blockage corrections for bluff-bodies in closed and open wind tunnels, In: *10th International Conference Wind Engineering, Copenhagen, June.*, pp. 1627-1634, 1999.
2) Flamand, O. : Rain-wind induced vibration of cable, In: *J. of Wind Engineering and Industrial Aerodynamics*, 57 (2-3), 353-340, 1995.
3) Flamand, O., Boujard, O. : A comparison between dry cylinder galloping and rain-wind induced excitation, In: *Proceeding of the 5th European & African Conference on Wind Engineering, Florence*, 2009
4) Georgakis, C.T., Koss, H.H., Ricciardelli, F. : Design specifications for a novel climatic wind tunnel for the testing of structural cables, In: *8th International Symposium on Cable Dynamics, Paris, France, September*, pp. 333–340, 2009.
5) Gimsing, N.J., Georgakis, C.T. : Cable Supported Bridges: Concept and Design, *3rd ed. John Wiley & Sons Ltd.*, 2011.
6) Hojo, T., Yamazaki, S., Okada, H. : Development of Lowdrag Aerodynamically Stable Cable with Indented Processing, Nippon Steel Corporation, *July (Special Issue on Steel Structure 82)*, URL /http://www.nsc.co.jp/en/tech/report/pdf/8203.pdfS, 2000.
7) Hojo, T., Yamazaki, S., Miyata, T., Yamada, H. : Development of aerodynamically stable cables for cable-stayed bridges having low resistance, *Bridges & Foundations Engineering 6*, 27–32, in Japanese, 1995
8) Kleissl, K., Georgakis, C.T. : Comparison of the aerodynamics of bridge cables with helical fillets and a pattern-indented surface in normal flow (a), In: *Proceedings of the 13th International Conference on Wind Engineering, Amsterdam*, 2011.
9) Kleissl, K., Georgakis, C.T. : Comparison of the aerodynamics of yawed bridge cables with helical fillets and a pattern-indented surface (b), In: *Proceedings of the 9th International Symposium on Cable Dynamics, Shanghai, China*, 2011.

[+1]celebur@byg.dtu.dk, [+2]cg@byg.dtu.k, [+3]svl@force.dk, [+4]philipp.egger@vsl.com

10) Matsumoto, M. : Observed behavior of proto type cable vibration and its generation mechanism, In: *Bridge Aerodynamics, Proceedings of the International Symposium on Advances in Bridge Aerodynamics*, pp. 189–211, 1998.
11) Matsumoto, M., Daito, Y., Kanamura, T., Shigemura, Y., Sakuma, S., Ishizaki, H. : Wind-induced vibration of cables of cable-stayed bridges, In: *J. of Wind Engineering and Industrial Aerodynamics*, 74-76, 1015 – 1027, 1998.
12) Miyata, Y., Yamada, H., Hojo, T. : Experimental study on aerodynamic characteristics of cables with patterned surface, In: *J. of Structural Engineering 40A (March)*, 1065–1076, 1994.
13) Miyata, T., Katsuchi, H., Tamura, Y. : Comprehensive discussion on structural control for wind-induced responses of bridges and buildings, In: *Wind Engineering into the 21st Century, Proceedings of the 10th International Conference on Wind Engineering*, vol. 1, pp. 487–494, 1999.
14) Nebres, J. V., Batill, S. M. : Flow about cylinders with helical surface protrusions, In: *30th AIAA Aerospace Sciences Meeting and Exhibit, Reno, Nevada 92 (0540)*, 1992.
15) Yagi, T., Okamoto, K., Sskski, I., Koroyasu, H., Liang, Z., Narita, S., Shirato, H. : Drag force reduction and aerodynamic stabilization of stay cables by modifying surface configurations, In: *The 21th Symposium on Wind Engineering, Tokyo, Japan.* In Japanese, 2010.
16) Zdravkovich, M. M. : Review and classification of various aerodynamic and hydrodynamic means for suppressing vortex shedding, In: *Journal of Wind Engineering and Industrial Aerodynamics 7 (2)*, 145 – 189, 1981.
17) Zdravkovich, M. M. : Reduction of effectiveness of means for suppressing wind-induced oscillation, In: *Engineering Structures 6 (4)*, 344 – 349, 1984.
18) Zdravkovich, M. M. : Flow around circular cylinders vol.1: fundamentals, *Oxford Science Publications*, 1997.

[+1]celebur@byg.dtu.dk, [+2]cg@byg.dtu.k, [+3]svl@force.dk, [+4]philipp.egger@vsl.com